General analytical theory of three-photon decays for hydrogenic ions with Coulomb Sturmian basis functions

Falone Fotsing ● and Moïse Godfroy Kwato Njock ●*
Centre for Atomic Molecular Physics and Quantum Optics (CEPAMOQ), Faculty of Science,
University of Douala, P.O. Box 8580 Douala, Cameroon

In this paper, we extend to three-photon radiative transitions in hydrogenic ions our fully relativistic multipole approach [Z. Bona *et al.*, Phys. Rev. A **89**, 022514 (2014)], which has proven so far to yield extremely accurate results for two-photon emission processes. Closed-form formulas of double and single differential frequency distributions as well as total emission probabilities are derived for arbitrary multipole channels by using the Dirac-Coulomb Sturmian functions of the first order. Two cases of atomic systems are considered in the study, namely, ions with a spinless nucleus and those with a nonzero nuclear spin to check the validity of the Bose-Einstein statistics for three-photon emission investigated by Zalialiutdinov *et al.* [J. Phys. B: At. Mol. Opt. Phys. **49**, 055001 (2016)]. In an effort to assess relativistic effects and the influence of the negative spectrum of the set of Dirac-Coulomb Sturmians, we formulate two nonrelativistic schemes that involve Schrödinger-Coulomb Sturmians, a transition operator with retardation, on one hand, and a transition operator in the long wavelength approximation, on the other hand. An application of these theories is made for the relativistic and nonrelativistic atomic transitions $2s_{1/2} \to 1s_{1/2}$, $2p_{1/2} \to 1s_{1/2}$, $2p_{3/2} \to 2s_{1/2}$ and $2s \to 1s$, $2p \to 1s$, respectively, with nuclear charge ranging from 1 to 100. Some of our numerical values are compared with the scarce data available in the literature and they enable us to draw inferences as to the improvements obtained with our approach, while the others are additional results that we provide as a further step for more investigations of three-photon decays.

I. INTRODUCTION

Since the advent of quantum mechanics, multiphoton processes have attracted special attention in various fields of physical sciences [1–7]. Starting with two-photon transitions in atomic systems, and notably with two-photon emission, theoretical studies can be traced back to the evaluation of the $2s \to 1s$ transition in atomic hydrogen, performed by Breit and Teller [8] from the seminal work of Goeppert-Mayer [9]. Since then, these works spawned subsequent developments and a strong debate. In recent years, for instance, quantum electrodynamics (QED) calculations of two-photon decay rates of H-like ions were carried out by a number of authors using several adequate techniques, among others by Goldman and Drake [10,11], Santos *et al.* [12], Amaro *et al.* [13], Jentschura and Surzhykov [14], Labzowsky *et al.* [15–17], and by us with our reliable and efficient Dirac-Coulomb Green Function (DCGF) scheme [18]. The exception being the predictions of Labzowsky *et al.* who used an approach based on the set of B-splines, the results of the other authors are closer to ours. For details see Ref. [18] in which the comparison and

discussion of all theoretical data obtained within the framework of these approaches are reflected.

From the above-mentioned investigations, it is evident that the chief difficulty in calculating the multiphoton emission stands in the correct evaluation of cumbersome summations over the possible unperturbed intermediate states of the system under consideration. To be specific for three-photon decays, two Green's functions are involved in the third-order amplitudes so that, on one hand, the derivation of their analytical expressions is tediously long, and on the other hand, they require considerable computational time and effort. That is why, to the best of our knowledge in this case, only the pioneering relativistic works of Zalialiutdinov *et al.* [19] were reported recently in the literature. Employing the B-spline method in the summations, these authors computed transition probabilities for $3E1$ and $3E2$ multipoles of $2s_{1/2}$, $2p_{1/2}$, and $2p_{3/2}$ states of H-like ions with a spinless nucleus and a nuclear charge up to 95. They also discussed the Bose-Einstein statistics (BES) for the transition $2p_{3/2} \to 1s_{1/2} + 3\gamma(E1)$ in the neutral hydrogen atom, and $2p_{3/2} \to 2s_{1/2} + 3\gamma(E1)$ in the hydrogenic ion $Z = 19$, both with a nonzero nuclear spin [20,21]. More information about the BES may be found in Refs. [22–26].

Because of its efficiency and success as far as two-photon radiative transitions (2-PRT) are concerned, our theory has emerged as a very useful and powerful tool of attack in QED calculations of atomic multiphon processes. Accordingly, it is expected that the DCGF scheme will also provide results with at least the same order of accuracy for three-photon radiative

---

*mkwato@yahoo.com

transitions (3-PRT). For this purpose we have extended our treatment by constructing a general analytical relativistic theory. Closed-form formulas obtained for differential frequency distributions are very convenient for computer calculations. In an effort to compare our numerical results with those available in Ref. [19], to assess relativistic effects and the influence of the negative spectrum of the set of Dirac-Coulomb Sturmians of first order, we derive two nonrelativistic approximations using Schrödinger-Coulomb Sturmian basis functions. In addition, it is also the purpose of the present contribution to provide new data for further studies.

The organization of this paper is as follows. Section II describes in detail the methods and calculations of our relativistic theory of three-photon decay rates. In Sec. III, nonrelativistic approaches are formulated by using first a transition operator expressed in the long wavelengths approximation (NRT-LWA), and second another one that incorporates retardation corrections (NRT-RC). Details on the angular coupling factors which intervene in the matrix elements are included in the Appendix. Section IV is devoted to the presentation of our numerical results. Finally, in Sec. V, we make some concluding remarks. Notice that atomic units (a.u.) and relativistic atomic units (r.a.u.) are used throughout.

II. RELATIVISTIC THEORY OF THREE-PHOTON RADIATIVE TRANSITIONS

In this section, we present the analytical relativistic theory of 3-PRT in hydrogenic ions, derived from our DCGF scheme previously developed for 2-PRT [18]. Since the general formalism is given in detail in that reference, we report here only the most important new formulas concerning 3-PRT for atomic systems considered below, namely, H-like ions with a spinless nucleus and those with a nonzero nuclear spin. Relativistic atomic units (r.a.u.) are used throughout this section and α stands for the fine structure constant. Their values for conversion in the tables are given in Refs. [18,27].

A. Emission rates for ions with a spinless nucleus

Within the framework of QED [28] and owing to our previous two-photon works, we formulate the general expression for three-photon decay rates in hydrogenic ions with a spinless nucleus for an arbitrary combination of multipoles and in the length gauge for electromagnetic potentials. The basic expression for the average double differential in energy decay rate may be written, as

$$\frac{d^2W}{d\omega_1 d\omega_2} = \frac{\alpha^3 \omega_1 \omega_2 \omega_3}{(2\pi)^5 (2j_i+1)} \sum_{m_i m_f} \sum_{(1),(2),(3)} |S[(3),(2),(1)] + 5 \text{ permutations}|^2, \quad (1)$$

where $S[(w),(v),(u)]$ is the third-order transition amplitude from an initial to a final atomic states

$$S[(w),(v),(u)] = \int_{\mathbb{R}^3} d\boldsymbol{r}_3 \int_{\mathbb{R}^3} d\boldsymbol{r}_2 \int_{\mathbb{R}^3} d\boldsymbol{r}_1 \Psi_f^\dagger(\boldsymbol{r}_3)$$
$$\times V[\boldsymbol{r}_3, \boldsymbol{k}_w,(w)] G_{E_2}(\boldsymbol{r}_3,\boldsymbol{r}_2) V[\boldsymbol{r}_2, \boldsymbol{k}_v,(v)]$$
$$\times G_{E_1}(\boldsymbol{r}_2,\boldsymbol{r}_1) V[\boldsymbol{r}_1, \boldsymbol{k}_u,(u)] \Psi_i(\boldsymbol{r}_1). \quad (2)$$

As is evident in Eq. (2), the numbers 1, 2, 3 stand for the vertexes of the Feynman diagram from which the three photons u, v, w are emitted, respectively. The notation (u) means $(\lambda_u L_u M_u)$ of the uth photon of frequency ω_u and wave vector $\boldsymbol{k}_u$, with $u=1,2,3$. λ_u, L_u, M_u stand for the photon multipole, angular momentum and its projection. We recall that terms with $\lambda_u=1$ and $\lambda_u=0$ are of electric and magnetic types, respectively. G_E represents the first-order DCGF with energy parameter E of the intermediate virtual states [29]. The one-body transition operator V denotes the interaction of the electron with the electromagnetic field [10]. Separating in the standard way the spin-angular and radial parts in matrix elements for the diagram (u,v,w), leads to

$$S[(w),(v),(u)] = (-i)^{L_w+L_v+L_u}(4\pi)^{3/2}$$
$$\times \sum_{j_1 j_2} B_{j_1 j_2}(w,v,u)\theta_{j_1 j_2}(w,v,u). \quad (3)$$

For computation purposes, it is convenient to express the radial integrals in a matrix form as

$$B_{j_1 j_2}(w,v,u) = \Delta_{j_1 j_2}(w,v,u)\langle \boldsymbol{U}_f^{(\lambda_w L_w)}(\omega_w)|\boldsymbol{\Gamma}^{(\lambda_v L_v)}(\omega_v)|$$
$$\times \boldsymbol{U}_i^{(\lambda_u L_u)}(\omega_u)\rangle, \quad (4)$$

where the elements of the vectors $|\boldsymbol{U}_i^{(\lambda L)}\rangle$ and $|\boldsymbol{U}_f^{(\lambda L)}\rangle$ and the matrix $\boldsymbol{\Gamma}^{(\lambda L)}$ are respectively given by

$$U_{i,n_1\kappa_1}^{(\lambda L)} = M_{n_1\kappa_1,n_i\kappa_i}^{(\lambda L)},$$
$$U_{f,n_2\kappa_2}^{(\lambda L)} = M_{n_f\kappa_f,n_2\kappa_2}^{(\lambda L)},$$
$$\Gamma_{n_2\kappa_2,n_1\kappa_1}^{(\lambda L)} = M_{n_2\kappa_2,n_1\kappa_1}^{(\lambda L)}. \quad (5)$$

It should be noted that transitions proceed through intermediate virtual states related to the quantum numbers (n_1,j_1,κ_1,m_1) and (n_2,j_2,κ_2,m_2) which form a complete set of states, including both positive and negative energies of the Dirac spectrum. The radial quantum numbers are such that $-\infty < n_2, n_1 < \infty$, while the Dirac angular quantum numbers κ_2 and κ_1 run over all possible integer values allowed by three-photon selection rules. The initial and final ionic bound states are defined by the quantum numbers (n_i,j_i,κ_i,m_i) and (n_f,j_f,κ_f,m_f) related to energies E_i and E_f, respectively. As for the angular couplings, they read

$$\Delta_{j_1 j_2}(w,v,u) = [j_f,j_2,j_1,j_i]^{1/2} \begin{pmatrix} j_f & L_w & j_2 \\ 1/2 & 0 & -1/2 \end{pmatrix} \begin{pmatrix} j_2 & L_v & j_1 \\ 1/2 & 0 & -1/2 \end{pmatrix} \begin{pmatrix} j_1 & L_u & j_i \\ 1/2 & 0 & -1/2 \end{pmatrix}, \quad (6)$$

$$\theta_{j_1 j_2}(w,v,u) = [j_2,j_1]^{1/2} \sum_{m_1 m_2}(-1)^\chi \begin{pmatrix} j_f & L_w & j_2 \\ -m_f & -M_w & m_2 \end{pmatrix} \begin{pmatrix} j_2 & L_v & j_1 \\ -m_2 & -M_v & m_1 \end{pmatrix} \begin{pmatrix} j_1 & L_u & j_i \\ -m_1 & -M_u & m_i \end{pmatrix}, \quad (7)$$

with $[a, b, \ldots, c] = (2a + 1)(2b + 1) \ldots (2c + 1)$ and $\chi = m_2 + m_1 + m_i - 1/2$. Our aim is to derive an analytical and simple expression for the double differential emission rate. This is accomplished after very lengthy manipulations, and finally we are able to transform Eq. (1) to the following general closed form:

$$\frac{d^2W}{dy_1 dy_2} = \frac{2\alpha^3 y_1 y_2 y_3 \omega_0^5}{\pi^2 (2j_i + 1)} \sum_{\text{all } \lambda L} \left\{ \sum_{k=1}^{5} \mathcal{P}_k \right\}, \tag{8}$$

where the first term stands for the direct partial contributions of the possible Feynman diagrams

$$\mathcal{P}_1 = \sum_{j_1 j_2} \{ |B_{j_1 j_2}(3, 2, 1)|^2 + 5 \text{ permutations} \}, \tag{9}$$

and the others contributions are cross terms

$$\mathcal{P}_2 = 2 \sum_{j_1 j_2} \left\{ B_{j_1 j_2}(3, 2, 1) \sum_{j_1'} \hat{K}^{(1)}_{j_1 j_1'}(2, 1) B^*_{j_1' j_2}(3, 1, 2) + B_{j_1 j_2}(1, 3, 2) \sum_{j_1'} \hat{K}^{(1)}_{j_1 j_1'}(3, 2) B^*_{j_1' j_2}(1, 2, 3) \right.$$

$$\left. + B_{j_1 j_2}(2, 1, 3) \sum_{j_1'} \hat{K}^{(1)}_{j_1 j_1'}(1, 3) B^*_{j_1' j_2}(2, 3, 1) \right\}, \tag{10}$$

$$\mathcal{P}_3 = 2 \sum_{j_1 j_2} \left\{ B_{j_1 j_2}(3, 2, 1) \sum_{j_2'} \check{K}^{(1)}_{j_2 j_2'}(3, 2) B^*_{j_1 j_2'}(2, 3, 1) + B_{j_1 j_2}(1, 3, 2) \sum_{j_2'} \check{K}^{(1)}_{j_2 j_2'}(1, 3) B^*_{j_1 j_2'}(3, 1, 2) \right.$$

$$\left. + B_{j_1 j_2}(2, 1, 3) \sum_{j_2'} \check{K}^{(1)}_{j_2 j_2'}(2, 1) B^*_{j_1 j_2'}(1, 2, 3) \right\}, \tag{11}$$

$$\mathcal{P}_4 = 2 \sum_{j_1 j_2 j_1' j_2'} \left[\hat{K}^{(1)}_{j_1 j_1'}(2, 1) \check{K}^{(2)}_{j_2 j_2'}(3, 1) B_{j_1 j_2}(3, 2, 1) B^*_{j_1' j_2'}(1, 3, 2) + \hat{K}^{(2)}_{j_1 j_1'}(3, 1) \check{K}^{(1)}_{j_2 j_2'}(3, 2) B_{j_1 j_2}(3, 2, 1) B^*_{j_1' j_2'}(2, 1, 3) \right.$$

$$+ \hat{K}^{(1)}_{j_1 j_1'}(3, 2) \check{K}^{(2)}_{j_2 j_2'}(1, 2) B_{j_1 j_2}(1, 3, 2) B^*_{j_1' j_2'}(2, 1, 3) + \hat{K}^{(1)}_{j_1 j_1'}(1, 2) \check{K}^{(2)}_{j_2 j_2'}(3, 2) B_{j_1 j_2}(3, 1, 2) B^*_{j_1' j_2'}(2, 3, 1)$$

$$\left. + \hat{K}^{(2)}_{j_1 j_1'}(3, 2) \check{K}^{(1)}_{j_2 j_2'}(3, 1) B_{j_1 j_2}(3, 1, 2) B^*_{j_1' j_2'}(1, 2, 3) + \hat{K}^{(1)}_{j_1 j_1'}(3, 1) \check{K}^{(2)}_{j_2 j_2'}(2, 1) B_{j_1 j_2}(2, 3, 1) B^*_{j_1' j_2'}(1, 2, 3) \right], \tag{12}$$

$$\mathcal{P}_5 = 2 \sum_{j_1 j_2 j_1' j_2'} [K_{j_1 j_2 j_1' j_2'}(3, 2, 1) B_{j_1 j_2}(3, 2, 1) B^*_{j_1' j_2'}(1, 2, 3) + K_{j_1 j_2 j_1' j_2'}(1, 3, 2) B_{j_1 j_2}(1, 3, 2) B^*_{j_1' j_2'}(2, 3, 1)$$

$$+ K_{j_1 j_2 j_1' j_2'}(2, 1, 3) B_{j_1 j_2}(2, 1, 3) B^*_{j_1' j_2'}(3, 1, 2)]. \tag{13}$$

Owing to the energy conservation requirement, we have

$$\omega_0 = E_i - E_f = \sum_{u=1}^{3} \omega_u, \quad \omega_u = y_u \omega_0, \quad 0 < y_u < 1. \tag{14}$$

y_u is the fraction of energy carried by the uth photon and ω_0 is the energy of the atomic transition. The spin-angular coupling coefficients $\hat{K}^{(1)}_{j_1 j_1'}$, $\hat{K}^{(2)}_{j_1 j_1'}$, $\check{K}^{(1)}_{j_2 j_2'}$, $\check{K}^{(2)}_{j_2 j_2'}$, $K_{j_1 j_2 j_1' j_2'}$ expressed in terms of $6j$ and $9j$ Wigner symbols are outlined in the Appendix.

B. Emission rates for ions with a nonzero nuclear spin

The hyperfine structure of the atomic levels is considered here by taking into account the nonzero nuclear spin $\boldsymbol{I}$ of the H-like ion. Accordingly, its total angular momentum is $\boldsymbol{F} = \boldsymbol{j} + \boldsymbol{I}$ with $|j - I| \leqslant F \leqslant j + I$. Thus, the matrix elements to be used in this case for 3-PRT between different hyperfine sublevels of different fine-structure levels can be obtained in

virtue of the Wigner-Eckart theorem, as

$$\langle \alpha_\sigma j_\sigma I_\sigma, F_\sigma M_\sigma | T^k_q | \alpha_\tau j_\tau I_\tau, F_\tau M_\tau \rangle$$

$$= \delta_{I_\sigma I_\tau} (-1)^{F_\sigma + F_\tau + j_\sigma + k + I - M_\sigma} [F_\sigma, F_\tau]^{1/2} \begin{pmatrix} F_\sigma & k & F_\tau \\ -M_\sigma & q & M_\tau \end{pmatrix}$$

$$\times \begin{Bmatrix} F_\sigma & k & F_\tau \\ j_\tau & I & j_\sigma \end{Bmatrix} \langle \alpha_\sigma j_\sigma \| T^k \| \alpha_\tau j_\tau \rangle. \tag{15}$$

The notation $I_\sigma = I_\tau = I$ comes from the Kronecker's symbol $\delta_{I_\sigma I_\tau}$. The reduced matrix element $\langle \alpha_\sigma j_\sigma \| T^k \| \alpha_\tau j_\tau \rangle$ was evaluated in Refs. [18,30,31]. By exploiting this result and following the same procedure, we arrive at

$$\frac{d^2 \widehat{W}}{dy_1 dy_2} = \frac{2\alpha^3 y_1 y_2 y_3 \omega_0^5}{\pi^2 (2F_i + 1)} \sum_{\text{all } \lambda L} \left\{ \sum_{k=1}^{5} \widehat{\mathcal{P}}_k \right\}, \tag{16}$$

where the terms $\widehat{\mathcal{P}}_k$ can be obtained from the formulas (9) to (13) by simple substitutions, namely, $\sum_{j_1 j_2} \rightarrow \sum_{j_1 j_2 F_1 F_2}$, $j \rightarrow F$ in the angular couplings coefficients $\hat{K}^{(i)}$, $\check{K}^{(i)}$, K, and

$B_{j_1 j_2} \rightarrow \mathcal{B}_{j_1 j_2 F_1 F_2}$ for the radial integrals.

$$\mathcal{B}_{j_1 j_2 F_1 F_2}(w, v, u) = B_{j_1 j_2}(w, v, u) \Lambda_{j_1 j_2 F_1 F_2}(w, v, u), \tag{17}$$

with

$$\Lambda_{j_1 j_2 F_1 F_2}(w, v, u) = [j_2, j_1]^{1/2} [F_f, F_2, F_1, F_i]^{1/2} \begin{Bmatrix} F_f & L_w & F_2 \\ j_2 & I & j_f \end{Bmatrix} \begin{Bmatrix} F_2 & L_v & F_1 \\ j_1 & I & j_2 \end{Bmatrix} \begin{Bmatrix} F_1 & L_u & F_i \\ j_i & I & j_1 \end{Bmatrix}. \tag{18}$$

From the $6j$ symbols in Eq. (18), we get the selection rules of the total angular momentum F_1 and F_2, i.e., $|F_i - L_u| \leqslant F_1 \leqslant F_i + L_u, |j_1 - I| \leqslant F_1 \leqslant j_1 + I, |F_2 - L_v| \leqslant F_1 \leqslant F_2 + L_v, |F_f - L_w| \leqslant F_2 \leqslant F_f + L_w, |j_2 - I| \leqslant F_2 \leqslant j_2 + I$.

III. NONRELATIVISTIC APPROACH OF THREE-PHOTON DECAYS

This section is devoted to derive explicitly the theory of 3-PRT in nonrelativistic hydrogenic ions. This will serve as a test for relativistic calculations, particularly for low nuclear charges, and to estimate retardation effects as well as the influence of the negative spectrum of the Dirac-Coulomb Sturmians. Only electric multipole are considered in what follows, i.e., $\lambda_u = 1 \equiv E$, $u = 1, 2, 3$. Atomic units (a.u.) are used throughout this section.

A. Spectral distribution with retardation

The nonrelativistic length form of the electric multipole transition operator which includes retardation, is defined as [28]

$$V_{LM}(\boldsymbol{r}, \omega) = -(-i)^L \left(\frac{4\pi\omega}{R}\right)^{1/2} \sqrt{\frac{L+1}{L}} j_L(\alpha\omega r) Y_{LM}^*(\hat{\boldsymbol{r}}). \tag{19}$$

j_L is the spherical Bessel function. The use of the Schrödinger-Coulomb representation of the Green function expressed by the partial wave decomposition [18,32–34], together with Eq. (19), yields the NRT-RC spectral distribution

$$\frac{d^2\widetilde{W}}{dy_1 dy_2} = \frac{2\alpha^3 y_1 y_2 y_3 \widetilde{\omega}_0^5}{\pi^2 (2\ell_i + 1)} \sum_{\text{all } L} \zeta_{L_1, L_2, L_3} \sum_{m_i m_f} \sum_{\text{all } M} \left| \widetilde{S}[(3), (2), (1)] + 5 \text{ permutations} \right|^2, \tag{20}$$

where

$$\zeta_{L_1, L_2, L_3} = \prod_{k=1}^{3} \frac{(L_k + 1)(2L_k + 1)}{L_k}, \quad \widetilde{\omega}_0 = \xi_i - \xi_f, \tag{21}$$

$$\widetilde{S}[(w), (v), (u)] = \sum_{\ell_1 \ell_2} \widetilde{B}_{\ell_1 \ell_2}(w, v, u) \widetilde{\theta}_{\ell_1 \ell_2}(w, v, u), \tag{22}$$

with

$$\widetilde{\theta}_{\ell_1 \ell_2}(w, v, u) = [\ell_1, \ell_2]^{1/2} \sum_{m_1 m_2} (-1)^{\widetilde{\chi}} \begin{pmatrix} \ell_f & L_w & \ell_2 \\ -m_f & -M_w & m_2 \end{pmatrix} \begin{pmatrix} \ell_2 & L_v & \ell_1 \\ -m_2 & -M_v & m_1 \end{pmatrix} \begin{pmatrix} \ell_1 & L_u & \ell_i \\ -m_1 & -M_u & m_i \end{pmatrix}, \tag{23}$$

$$\widetilde{B}_{\ell_1 \ell_2}(w, v, u) = \widetilde{\Delta}_{\ell_1 \ell_2}(w, v, u) \langle \widetilde{U}_f^{(\lambda_w L_w)}(\omega_w) | \widetilde{\boldsymbol{\Gamma}}^{(\lambda_v L_v)}(\omega_v) | \widetilde{U}_i^{(\lambda_u L_u)}(\omega_u) \rangle, \tag{24}$$

$$\widetilde{\Delta}_{\ell_1 \ell_2}(w, v, u) = [\ell_f, \ell_2, \ell_1, \ell_i]^{1/2} \begin{pmatrix} \ell_f & L_w & \ell_2 \\ 0 & 0 & 0 \end{pmatrix} \begin{pmatrix} \ell_2 & L_v & \ell_1 \\ 0 & 0 & 0 \end{pmatrix} \begin{pmatrix} \ell_1 & L_u & \ell_i \\ 0 & 0 & 0 \end{pmatrix}, \tag{25}$$

and $\widetilde{\chi} = m_2 + m_1 + m_i$. As in the previous section, the vectors $\widetilde{U}_f^{(L)}, \widetilde{U}_i^{(L)}$ and the matrix $\widetilde{\boldsymbol{\Gamma}}^{(L)}$ are given by

$$\widetilde{U}_{f,n_2\kappa_2}^{(L)} = \eta_{n_2\ell_2} \widetilde{M}_{n_f\ell_f, n_2\ell_2}^{(L)}, \quad \widetilde{U}_{i,n_1\kappa_1}^{(L)} = \eta_{n_1\ell_1} \widetilde{M}_{n_1\ell_1, n_i\ell_i}^{(L)}, \quad \widetilde{\Gamma}_{n_2\ell_2, n_1\ell_1}^{(L)} = \widetilde{M}_{n_2\ell_2, n_1\ell_1}^{(L)}, \tag{26}$$

while the factor $\eta_{n\ell}$ and the radial integrals take the form

$$\eta_{n\ell} = \frac{n + \ell + 1}{\lambda[\lambda(n + \ell + 1) - Z]}, \quad \widetilde{M}_{n'\ell', n\ell}^{(L)}(\omega) = \int_0^\infty dr \, S_{n'\ell'}(r) j_L(\alpha\omega r) S_{n\ell}(r). \tag{27}$$

$\lambda = \sqrt{-2\xi}$ and $S_{n\ell}(r)$ are the Schrödinger-Coulomb radial Sturmian functions [18]. It should be noted that the intermediate virtual states are characterized by the quantum numbers (n_1, ℓ_1, m_1) and (n_2, ℓ_2, m_2). They follow through selection rules for given initial and final atomic states. The radial quantum numbers in this case are assumed to be nonnegative. After some

calculations, one can establish Eq. (20) in the final form

$$\frac{d^2\widetilde{W}}{dy_1 dy_2} = \frac{2\alpha^3 y_1 y_2 y_3 \widetilde{\omega}_0^5}{\pi^2(2\ell_i+1)} \sum_{L_1 L_2 L_3} \zeta_{L_1,L_2,L_3} \left\{ \sum_{k=1}^{5} \widetilde{\mathcal{P}}_k \right\}, \tag{28}$$

$$\widetilde{\mathcal{P}}_1 = \sum_{\ell_1 \ell_2} \{|\widetilde{B}_{\ell_1 \ell_2}(3,2,1)|^2 + 5\,\text{permutations}\}, \tag{29}$$

$$\widetilde{\mathcal{P}}_2 = -2 \sum_{\ell_1 \ell_2} \left\{ \widetilde{B}_{\ell_1 \ell_2}(3,2,1) \sum_{\ell_1'} \hat{K}^{(1)}_{\ell_1 \ell_1'}(2,1) \widetilde{B}^*_{\ell_1' \ell_2}(3,1,2) + \widetilde{B}_{\ell_1 \ell_2}(1,3,2) \sum_{\ell_1'} \hat{K}^{(1)}_{\ell_1 \ell_1'}(3,2) \widetilde{B}^*_{\ell_1' \ell_2}(1,2,3) \right.$$

$$\left. + \widetilde{B}_{\ell_1 \ell_2}(2,1,3) \sum_{\ell_1'} \hat{K}^{(1)}_{\ell_1 \ell_1'}(1,3) \widetilde{B}^*_{\ell_1' \ell_2}(2,3,1) \right\}, \tag{30}$$

$$\widetilde{\mathcal{P}}_3 = -2 \sum_{\ell_1 \ell_2} \left\{ \widetilde{B}_{\ell_1 \ell_2}(3,2,1) \sum_{\ell_2'} \check{K}^{(1)}_{\ell_2 \ell_2'}(3,2) \widetilde{B}^*_{\ell_1 \ell_2'}(2,3,1) + \widetilde{B}_{\ell_1 \ell_2}(1,3,2) \sum_{\ell_2'} \check{K}^{(1)}_{\ell_2 \ell_2'}(1,3) \widetilde{B}^*_{\ell_1 \ell_2'}(3,1,2) \right.$$

$$\left. + \widetilde{B}_{\ell_1 \ell_2}(2,1,3) \sum_{\ell_2'} \check{K}^{(1)}_{\ell_2 \ell_2'}(2,1) \widetilde{B}^*_{\ell_1 \ell_2'}(1,2,3) \right\}, \tag{31}$$

$$\widetilde{\mathcal{P}}_4 = 2 \sum_{\ell_1 \ell_2 \ell_1' \ell_2'} \left[\hat{K}^{(1)}_{\ell_1 \ell_1'}(2,1) \check{K}^{(2)}_{\ell_2 \ell_2'}(3,1) \widetilde{B}_{\ell_1 \ell_2}(3,2,1) \widetilde{B}^*_{\ell_1' \ell_2'}(1,3,2) + \hat{K}^{(2)}_{\ell_1 \ell_1'}(3,1) \check{K}^{(1)}_{\ell_2 \ell_2'}(3,2) \widetilde{B}_{\ell_1 \ell_2}(3,2,1) \widetilde{B}^*_{\ell_1' \ell_2'}(2,1,3) \right.$$

$$+ \hat{K}^{(1)}_{\ell_1 \ell_1'}(3,2) \check{K}^{(2)}_{\ell_2 \ell_2'}(1,2) \widetilde{B}_{\ell_1 \ell_2}(1,3,2) \widetilde{B}^*_{\ell_1' \ell_2'}(2,1,3) + \hat{K}^{(1)}_{\ell_1 \ell_1'}(1,2) \check{K}^{(2)}_{\ell_2 \ell_2'}(3,2) \widetilde{B}_{\ell_1 \ell_2}(3,1,2) \widetilde{B}^*_{\ell_1' \ell_2'}(2,3,1)$$

$$\left. + \hat{K}^{(2)}_{\ell_1 \ell_1'}(3,2) \check{K}^{(1)}_{\ell_2 \ell_2'}(3,1) \widetilde{B}_{\ell_1 \ell_2}(3,1,2) \widetilde{B}^*_{\ell_1' \ell_2'}(1,2,3) + \hat{K}^{(1)}_{\ell_1 \ell_1'}(3,1) \check{K}^{(2)}_{\ell_2 \ell_2'}(2,1) \widetilde{B}_{\ell_1 \ell_2}(2,3,1) \widetilde{B}^*_{\ell_1' \ell_2'}(1,2,3) \right], \tag{32}$$

$$\widetilde{\mathcal{P}}_5 = 2 \sum_{\ell_1 \ell_2 \ell_1' \ell_2'} \left[K_{\ell_1 \ell_2 \ell_1' \ell_2'}(3,2,1) \widetilde{B}_{\ell_1 \ell_2}(3,2,1) \widetilde{B}^*_{\ell_1' \ell_2'}(1,2,3) + K_{\ell_1 \ell_2 \ell_1' \ell_2'}(1,3,2) \widetilde{B}_{\ell_1 \ell_2}(1,3,2) \widetilde{B}^*_{\ell_1' \ell_2'}(2,3,1) \right.$$

$$\left. + K_{\ell_1 \ell_2 \ell_1' \ell_2'}(2,1,3) \widetilde{B}_{\ell_1 \ell_2}(2,1,3) \widetilde{B}^*_{\ell_1' \ell_2'}(3,1,2) \right], \tag{33}$$

where the expressions $\hat{K}^{(1)}_{\ell_1 \ell_1'}, \hat{K}^{(2)}_{\ell_1 \ell_1'}, \check{K}^{(1)}_{\ell_2 \ell_2'}, \check{K}^{(2)}_{\ell_2 \ell_2'}, K_{\ell_1 \ell_2 \ell_1' \ell_2'}$ are analogously defined from their relativistic counterparts, namely that they are obtained from the substitutions $j_\nu \to \ell_\nu$, $j_\nu' \to \ell_\nu'$ in Eqs. (A14) to (A18).

B. Long wavelengths approximation of the spectral distribution

Within the long wavelength approximation, i.e., by retaining only the leading retardation term in the series expansion of the spherical Bessel function [35] in the nonrelativistic transition operator (19), it becomes

$$V^{(\text{LWA})}_{\text{LM}}(\boldsymbol{r},\omega) = -(-i)^L \left(\frac{4\pi\omega}{R}\right)^{1/2} \sqrt{\frac{L+1}{L}} \frac{(\alpha\omega)^L}{(2L+1)!!} r^L Y^*_{\text{LM}}(\hat{\boldsymbol{r}}). \tag{34}$$

By inserting this expression in the transition amplitudes and after some manipulations, we get the formula of the NRT-LWA spectral distribution as follows:

$$\frac{d^2\widetilde{W}^{(\text{LWA})}}{dy_1 dy_2} = \frac{2\widetilde{\omega}_0^2}{\pi^2(2\ell_i+1)} \sum_{L_1 L_2 L_3} \alpha^{2L_1+2L_2+2L_3+3} \zeta^{(\text{LWA})}_{L_1,L_2,L_3} \omega_1^{2L_1+1} \omega_2^{2L_2+1} \omega_3^{2L_3+1} \left\{ \sum_{k=1}^{5} \widetilde{\mathcal{P}}^{(\text{LWA})}_k \right\}, \tag{35}$$

$$\zeta^{(\text{LWA})}_{L_1,L_2,L_3} = \prod_{k=1}^{3} \frac{(L_k+1)(2L_k+1)}{L_k[(2L_k+1)!!]^2}. \tag{36}$$

The passage from $\widetilde{\mathcal{P}}_k$ to $\widetilde{\mathcal{P}}^{(\text{LWA})}_k$ is implemented with the use of radial integrals

$$q_{\ell_1 \ell_2}(w,v,u) = \widetilde{\Delta}(w,v,u) I_{\ell_1 \ell_2}(\xi_2,\xi_1;w,v,u), \tag{37}$$

where

$$I_{\ell_1 \ell_2}(\xi_2,\xi_1;w,v,u) = \int_0^\infty dr_3 \int_0^\infty dr_2 \int_0^\infty dr_1 r_3^{L_w+1} r_2^{L_v} r_1^{L_u+1} P_f(r_3) g_{\ell_2}(\xi_2,r_3,r_2) g_{\ell_1}(\xi_1,r_2,r_1) P_i(r_1). \tag{38}$$

Let us now apply the spectral formulas (35) to (38) to the transition $2s \rightarrow 1s + 3\gamma(E2)$ whose intermediate virtual states are $n_2 d\, n_1 d$. The integral (38) can be evaluated by the following general formula [36]:

$$
\begin{aligned}
D_{\ell_1 \ell_2}(m; p, s, q; \lambda_2, \lambda_1) &= Z^m \int_0^\infty dr_3 \int_0^\infty dr_2 \int_0^\infty dr_1 e^{-Z(r_3 + r_1/2)} r_3^p r_2^s r_1^q g_{\ell_2}(\xi_2, r_3, r_2) g_{\ell_1}(\xi_1, r_2, r_1) \\
&= C_{\ell_1 \ell_2}^{\nu_1 \nu_2} \sum_{n_2=0}^\infty \sum_{n_1=0}^\infty \frac{(n_2 + 2\ell_2 + 1)!}{(n_2 + \ell_2 + 1 - \nu_2) n_2!} \frac{(n_1 + 2\ell_1 + 1)!}{(n_1 + \ell_1 + 1 - \nu_1) n_1!} \\
&\quad \times {}_2F_1\left(-n_2, \ell_2 + p + 2; 2\ell_2 + 2; \frac{2}{\nu_2 + 1}\right) \\
&\quad \times {}_2F_1\left(-n_1; \ell_1 + q + 2; 2\ell_1 + 2; \frac{4}{\nu_1 + 1}\right) K_{\ell_1 \ell_2}^{n_1 n_2}(\nu_2, \nu_1),
\end{aligned}
\tag{39}
$$

where

$$
C_{\ell_1 \ell_2}^{\nu_1 \nu_2} = \frac{2^{2\ell_2 + 3\ell_1 + q + 6} \nu_2^{\ell_1 + p + s + 4} \nu_1^{\ell_2 + q + s + 4}}{(\nu_2 + 1)^{\ell_2 + p + 2} (\nu_2 + \nu_1)^{\ell_2 + \ell_1 + s + 3} (\nu_1 + 2)^{\ell_1 + q + 2}} \frac{(\ell_2 + p + 1)!(\ell_1 + q + 1)!}{Z^{p + s + q - m + 5}[(2\ell_2 + 1)!(2\ell_1 + 1)!]^2},
\tag{40}
$$

$$
K_{\ell_1 \ell_2}^{n_1 n_2}(\nu_2, \nu_1) = \int_0^\infty dx\, e^{-x} x^{\ell_2 + \ell_1 + s + 2} Q_{\ell_1 \ell_2}^{n_1 n_2}(x),
\tag{41}
$$

$$
Q_{\ell_1 \ell_2}^{n_1 n_2}(x) = {}_1F_1\left(-n_2; 2\ell_2 + 2; \frac{2\nu_1 x}{\nu_2 + \nu_1}\right) {}_1F_1\left(-n_1; 2\ell_1 + 2; \frac{2\nu_2 x}{\nu_2 + \nu_1}\right),
\tag{42}
$$

$$
\nu_k = \frac{\sqrt{-2\xi_k}}{Z}, \quad k = 1, 2.
\tag{43}
$$

${}_2F_1$ and ${}_1F_1$ are the Gauss and confluent hypergeometric functions [35], respectively. Since $Q_{\ell_1 \ell_2}^{n_1 n_2}(x)$ is a polynomial of degree $n_1 + n_2$ in x, a simple Gauss-Laguerre quadrature is well adapted to a highly accurate calculation of Eq. (41). With these expressions, the spectral distribution takes the final form

$$
\frac{d^2 \widetilde{W}^{(\mathrm{LWA})}}{dy_1 dy_2} = \frac{3^{14}}{2^{21} 5^8 7\pi^2} \alpha(\alpha Z)^{14} y_1^5 y_2^5 y_3^5 \left\{ \sum_{k=1}^6 \left[\widetilde{I}_{22}\left(\nu_2^{(k)}, \nu_1^{(k)}\right)\right]^2 + 2 \sum_{j=1}^5 \widetilde{I}_{22}\left(\nu_2^{(j)}, \nu_1^{(j)}\right) \sum_{k=j+1}^6 \widetilde{I}_{22}\left(\nu_2^{(k)}, \nu_1^{(k)}\right) \right\},
\tag{44}
$$

where

$$
\begin{aligned}
\widetilde{I}_{22}(b, a) &= \frac{b^{11} a^{11}}{(b+1)^7 (b+a)^9 (a+2)^7} \sum_{n_2=0}^\infty \sum_{n_1=0}^\infty \frac{(n_2 + 5)!}{n_2!(n_2 + 3 - b)} \frac{(n_1 + 5)!}{n_1!(n_1 + 3 - a)} {}_2F_1\left(-n_2, 7; 6; \frac{2}{b+1}\right) \\
&\quad \times \left[{}_2F_1\left(-n_1, 7; 6; \frac{4}{a+2}\right) - \frac{7a}{a+2} {}_2F_1\left(-n_1, 8; 6; \frac{4}{a+2}\right)\right] \widetilde{K}_{22}(b, a),
\end{aligned}
\tag{45}
$$

$$
\widetilde{K}_{22}(b, a) = \int_0^\infty dx\, e^{-x} x^8 {}_1F_1\left(-n_2; 6; \frac{2ax}{b+a}\right) {}_1F_1\left(-n_1; 6; \frac{2bx}{b+a}\right).
\tag{46}
$$

The pairs $(\nu_2^{(k)}, \nu_1^{(k)})$ refer to the Feynman diagrams $(k) \equiv (u, v, w)$, $k = 1, \ldots, 6$. They are such that

$$
\nu_1^{(k)} = \frac{2}{\sqrt{1 + 3y_u}}, \quad \nu_2^{(k)} = \frac{2}{\sqrt{4 - 3y_w}}.
\tag{47}
$$

Performing the evaluation of the total decay rate

$$
\widetilde{W}^{(\mathrm{LWA})} = \frac{1}{3!} \int_0^1 \int_0^1 \left(\frac{d^2 \widetilde{W}^{(\mathrm{LWA})}}{dy_1 dy_2}\right) dy_1 dy_2,
\tag{48}
$$

we get

$$
2s \rightarrow 1s + 3\gamma(E2): \ \widetilde{W}^{(\mathrm{LWA})}(3E2) = 3.469\,252\,162\,7 \times 10^{-12} \alpha(\alpha Z)^{14}.
\tag{49}
$$

TABLE I. Virtual states allowed in the multipole contributions included in calculations of relativistic three-photon decay rates with a spinless nucleus for the $2s_{1/2} \to 1s_{1/2}$ and $2p_{1/2} \to 1s_{1/2}$ transitions, and nonrelativistic three-photon decay rates for the $2s \to 1s$ and $2p \to 1s$ transitions.

Multipoles	Virtual states		Multipoles	Virtual states	
	$2s_{1/2} \to 1s_{1/2}$	$2s \to 1s$		$2p_{1/2} \to 1s_{1/2}$	$2p \to 1s$
$3E2$	$n_2 d_{3/2}\, n_1 d_{3/2},\ n_2 d_{3/2}\, n_1 d_{5/2},$	$n_2 d\, n_1 d$	$3E1$	$n_2 p_{1/2}\, n_1 s_{1/2},\ n_2 p_{1/2}\, n_1 d_{3/2},$	$n_2 p\, n_1 s,\ n_2 p\, n_1 d$
	$n_2 d_{5/2}\, n_1 d_{3/2},\ n_2 d_{5/2}\, n_1 d_{5/2}$			$n_2 p_{3/2}\, n_1 s_{1/2},\ n_2 p_{3/2}\, n_1 d_{3/2}$	
$2E1E2$	$n_2 p_{1/2}\, n_1 p_{3/2},\ n_2 p_{1/2}\, n_1 d_{3/2},$	$n_2 p\, n_1 p,\ n_2 p\, n_1 d,$	$2E2E1$	$n_2 p_{1/2}\, n_1 p_{3/2},\ n_2 p_{1/2}\, n_1 f_{5/2},$	$n_2 p\, n_1 p,\ n_2 p\, n_1 f,$
	$n_2 p_{3/2}\, n_1 p_{1/2},\ n_2 p_{3/2}\, n_1 p_{3/2},$	$n_2 d\, n_1 p$		$n_2 p_{3/2}\, n_1 p_{3/2},\ n_2 p_{3/2}\, n_1 f_{5/2},$	$n_2 d\, n_1 s,\ n_2 d\, n_1 p,$
	$n_2 p_{3/2}\, n_1 d_{3/2},\ n_2 p_{3/2}\, n_1 d_{5/2},$			$n_2 d_{3/2}\, n_1 s_{1/2},\ n_2 d_{3/2}\, n_1 p_{3/2},$	$n_2 d\, n_1 d,\ n_2 d\, n_1 f$
	$n_2 d_{3/2}\, n_1 p_{1/2},\ n_2 d_{3/2}\, n_1 p_{3/2},$			$n_2 d_{3/2}\, n_1 d_{3/2},\ n_2 d_{3/2}\, n_1 f_{5/2},$	
	$n_2 d_{5/2}\, n_1 p_{3/2}$			$n_2 d_{5/2}\, n_1 s_{1/2},\ n_2 d_{5/2}\, n_1 p_{3/2},$	
				$n_2 d_{5/2}\, n_1 d_{3/2},\ n_2 d_{5/2}\, n_1 f_{5/2}$	

We carried out in the same way calculations for three others transitions and obtained the formulas

$$2p \to 1s + 3\gamma(E1): \quad \widetilde{W}^{(\text{LWA})}(3E1) = 4.816\,308\,365\,9 \times 10^{-6}\, \alpha(\alpha Z)^8, \tag{50}$$

$$2s \to 1s + 2\gamma(E1) + \gamma(E2): \quad \widetilde{W}^{(\text{LWA})}(2E1E2) = 1.390\,521\,835\,3 \times 10^{-7}\, \alpha(\alpha Z)^{10}, \tag{51}$$

$$2p \to 1s + 2\gamma(E2) + \gamma(E1): \quad \widetilde{W}^{(\text{LWA})}(2E2E1) = 1.657\,122\,982\,3 \times 10^{-9}\, \alpha(\alpha Z)^{12}. \tag{52}$$

IV. COMPUTATIONAL RESULTS

The formulas derived above enable us to assess the effectiveness of our DCGF fully relativistic approach to a large selection of hydrogenic ions with nuclear charge Z ranging from 1 to 100 for certain well-defined electric transitions. Prior to the presentation of our numerical results and the comparison withthose of Zalialiutdinov *et al.* [19], some introductory statements are in order.

First, let us extend the well-known standard spectral distribution formula introduced by Spitzer and Greenstein [37] to three-photon emission spectra in the form

$$\frac{d^2 W}{dy_1 dy_2} = \frac{3^3}{2^{15}} \alpha \mathcal{Z}^q \psi(Z, y_1, y_2), \quad \mathcal{Z} = \alpha Z, \tag{53}$$

where the variables y_1 and y_2 are the fractions of energy carried by two of the three photons. From Eqs. (49) to (52), the multipoles $3E1$, $2E1E2$, $2E2E1$, and $3E2$ scale as $q = 8$, 10, 12 and 14, respectively. By integrating Eq. (53), one easily obtains the single differential probability and the total rate

$$\frac{dW}{dy} = \frac{3^3}{2^{15}} \alpha \mathcal{Z}^q \varphi(Z, y), \quad W = \alpha \mathcal{Z}^q \phi(Z), \tag{54}$$

respectively, where the variable y is the fraction of energy carried by one of the photons. It should be noted that the integrations over y_1 and y_2 are performed by means of a Gauss-Legendre quadrature [35].

Second, in the sums over the radial quantum numbers n_1 and n_2 occurring in equations of Secs. II and III, a finite expansion length $n_{\max}$ is used to obtain converged values. In the computations, we focus our attention on $\widetilde{W}$ and W, W_+ corresponding to the full $-n_{\max} \leqslant n_1, n_2 \leqslant n_{\max}$ and the

nonnegative $0 \leqslant n_1, n_2 \leqslant n_{\max}$ parts of the Dirac Sturmians basis, respectively.

Finally, let

$$d_1(\%) = 100 \times \frac{|\widetilde{W}^{(\text{LWA})} - W^{(\text{OTD})}|}{\widetilde{W}^{(\text{LWA})}},$$

$$d_2(\%) = 100 \times \frac{|W - W^{(\text{ZSL})}|}{W}, \tag{55}$$

be a measure of the difference, on one hand, between the nonrelativistic results in the long wavelengths approximation $\widetilde{W}^{(\text{LWA})}$ and the other theoretical data $W^{(\text{OTD})} \equiv W$, W_+, $\widetilde{W}$, and $W^{(\text{ZSL})}$ from the scheme denoted hereafter ZSL (Ref. [19]), and on the other hand, between our fully relativistic results considered as reference numbers and those of ZSL. With these useful tools we are now able to evaluate and adequately analyze three-photon decay rates of the selected $2s_{1/2}$, $2p_{1/2}$, and $2p_{3/2}$ atomic states investigated in this paper.

In Table I are listed the allowed virtual states involved in the summations of Eqs. (8), (16), (28), and (35) for the multipole decay channels considered here. They are dipole and quadrupole moments of each photon field, and all of electric type, namely, $3E1$, $3E2$, $2E1E2$, and $2E2E1$. It is obvious that when the moments of photons are not identical, the number of intermediate states increases rapidly especially in the relativistic case. This leads to tediously long calculations, and if one is not careful significant roundoff errors can occur. That is why great care has been exercised in evaluating radial integrals and the most crucial parameter $n_{\max} = 30$ has been used to reach the full convergence and the gauge (velocity and length) invariance of our results.

The partial three-photon decay rates of $3E1$ and $3E2$ multipoles for the transitions $2p_{1/2} \to 1s_{1/2}$ and $2s_{1/2} \to 1s_{1/2}$ are presented in Table II. Plots of percentage differences d_1

TABLE II. Three-photon decay rates in s^{-1} of combinations of $3E1$ and $3E2$ multipoles for the transitions $2p_{1/2} \to 1s_{1/2}$ and $2s_{1/2} \to 1s_{1/2}$, respectively, as a function of the nuclear charge. First entry: W; second entry: W_+; third entry: W_-; fourth entry: $W_{vel}^{(ZSL)}$ (Zalialiutdinov et $al.$ [19]); fifth entry: $W_{len}^{(ZSL)}$ (Zalialiutdinov et $al.$ [19]); sixth entry: $\widetilde{W}$; seventh entry: $\widetilde{W}^{(LWA)}$. Powers of ten are given in parentheses.

Z	W(3E1)	W(3E2)	Z	W(3E1)	W(3E2)	Z	W(3E1)	W(3E2)
1	1.168349(−8)	1.270639(−27)	35	2.522157(4)	5.100624(−6)	70	5.605106(6)	7.562072(−2)
	1.168344(−8)	1.270627(−27)		2.509935(4)	5.042402(−6)		5.481418(6)	7.191555(−2)
	8.657862(−32)	1.218649(−49)		4.587387(−7)	1.373462(−15)		3.355831(−2)	6.501112(−8)
	1.168620(−8)	1.284270(−27)		–	–		5.579235(6)	7.601921(−2)
	1.168632(−8)	1.284254(−27)		–	–		5.579255(6)	7.602718(−2)
	1.168367(−8)	1.270839(−27)		2.574487(4)	5.113693(−6)		6.176422(6)	7.698558(−2)
	1.168388(−8)	1.270869(−27)		2.631065(4)	5.260819(−6)		6.735525(6)	8.619325(−2)
5	4.560170(−3)	7.747346(−18)	40	7.242774(4)	3.287441(−5)	75	9.435201(6)	1.944611(−1)
	4.559737(−3)	7.745571(−18)		7.196334(4)	3.276170(−5)		9.189500(6)	1.833669(−1)
	1.322087(−20)	2.904537(−34)		3.901737(−6)	3.148102(−14)		1.035105(−1)	2.813930(−7)
	4.561173(−3)	7.833773(−18)		7.237156(4)	3.306380(−5)		–	–
	4.561219(−3)	7.833681(−18)		7.237208(4)	3.307976(−5)		–	–
	4.561990(−3)	7.752272(−18)		7.442873(4)	3.287441(−5)		1.059018(7)	1.989218(−1)
	4.564016(−3)	7.756767(−18)		7.657149(4)	3.411462(−5)		1.169707(7)	2.264427(−1)
10	1.164449	1.267718(−13)	45	1.829930(5)	1.685837(−4)	80	1.526970(7)	4.695684(−1)
	1.164006	1.266555(−13)		1.814865(5)	1.652729(−4)		1.480459(7)	4.389944(−1)
	8.685674(−16)	1.226286(−27)		2.606695(−5)	6.230732(−13)		3.010389(−1)	1.413162(−6)
	1.164659	1.281043(−13)		–	–		1.514879(7)	0.470047
	1.164670	1.284925(−13)		–	–		1.514883(7)	0.470080
	1.166314	1.267926(−13)		1.895365(5)	1.693290(−4)		1.750731(7)	4.823789(−1)
	1.168388	1.270869(−13)		1.964659(5)	1.774500(−4)		1.960230(7)	5.589340(−1)
15	2.971733(1)	3.689464(−11)	50	4.177085(5)	7.272263(−4)	85	2.385144(7)	1.067271
	2.969177(1)	3.681844(−11)		4.133876(5)	7.101204(−4)		2.300361(7)	9.864567(−1)
	5.727330(−13)	9.452561(−24)		1.441539(−4)	6.986868(−12)		7.992066(−1)	1.782239(−5)
	–	–		4.170711(5)	7.335633(−4)		–	–
	–	–		4.170735(5)	7.337452(−4)		–	–
	2.982508(1)	3.690737(−11)		4.366196(5)	7.321130(−4)		2.802626(7)	1.106154
	2.994451(1)	3.710038(−11)		4.564016(5)	7.756767(−4)		3.183747(7)	1.306068
20	2.950721(2)	2.061505(−9)	55	8.777790(5)	2.724497(−3)	90	3.606051(7)	2.308361
	2.946181(2)	2.053907(−9)		8.666009(5)	2.644430(−3)		3.457417(7)	2.108665
	5.735036(−11)	5.817424(−21)		6.523573(−4)	6.934832(−11)		2.031121	5.844450(−5)
	2.950782(2)	2.082775(−9)		–	–		3.554091(7)	2.304994
	2.950754(2)	2.087035(−9)		–	–		3.554098(7)	2.305110
	2.969901(2)	2.062977(−9)		9.272884(5)	2.746773(−3)		4.360108(7)	2.413735
	2.991074(2)	2.082191(−9)		9.783374(5)	2.945631(−3)		5.029528(7)	2.907340
25	1.745222(3)	4.661210(−8)	60	1.721858(6)	9.067125(−3)	95	5.288051(7)	4.766324
	1.740995(3)	4.634245(−8)		1.695238(6)	8.738897(−3)		5.036480(7)	4.297233
	2.033998(−9)	7.194352(−19)		2.681234(−3)	6.323082(−10)		5.431575	4.578344(−4)
	–	–		1.717285(6)	9.129899(−3)		5.182120(7)	4.744875
	–	–		1.717293(6)	9.131310(−3)		5.182120(7)	4.745083
	1.763144(3)	4.666286(−8)		1.841256(6)	9.164668(−3)		6.611811(7)	5.038400
	1.782819(3)	4.734355(−8)		1.962443(6)	9.959057(−3)		7.751326(7)	6.197709
30	7.432853(3)	5.943212(−7)	65	3.186122(6)	2.731937(−2)	100	7.535322(7)	9.432437
	7.406680(3)	5.893471(−7)		3.126788(6)	2.618000(−2)		7.119085(7)	8.379830
	3.860289(−8)	4.039676(−17)		1.136066(−2)	1.024228(−8)		1.229039(1)	1.942871(−3)
	7.430658(3)	6.001701(−7)		–	–		–	–
	7.430721(3)	6.008097(−7)		–	–		–	–
	7.544301(3)	5.953116(−7)		3.454806(6)	2.770444(−2)		9.798032(7)	1.010548(1)
	7.665795(3)	6.078526(−7)		3.723008(6)	3.054131(−2)		1.168388(8)	1.270869(1)

and d_2, and normalized integrated decay rates derived from these numbers are displayed against Z in Fig. 1. When cross-examining this figure together with the table, a few relevant features become apparent, including the following.

(i) Figures 1(a) and 1(e) clearly depict that the ZSL scheme is in error for the $3E2$ channel. Its curves not only exhibit an irregular behavior, but also reveal a large discrepancy with the nonrelativistic values for the ions in the
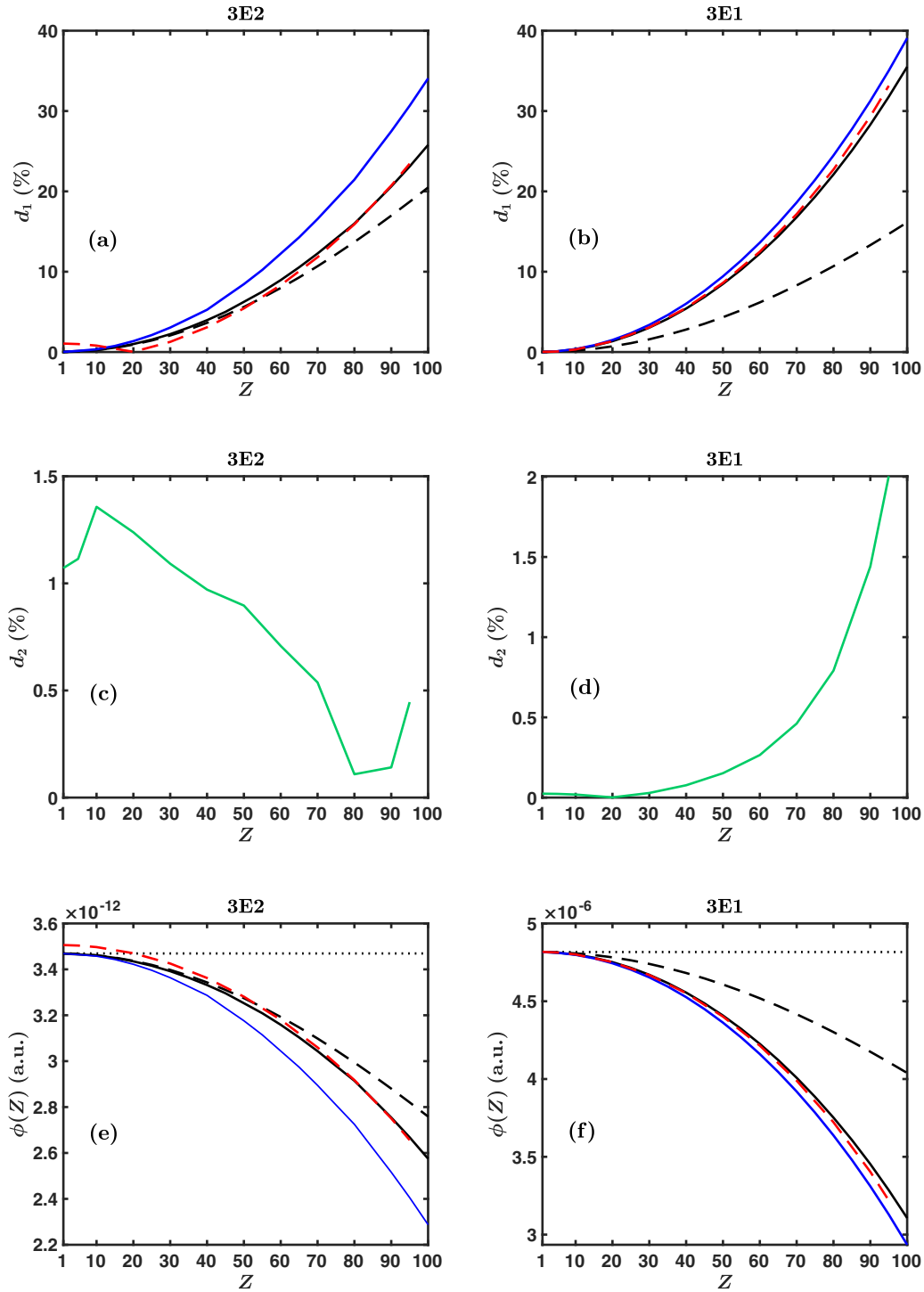
FIG. 1. An illustration of the behavior of the percentage differences and the normalized integrated decay rate for the transitions $2s_{1/2} \rightarrow 1s_{1/2}(3E2)$ and $2p_{1/2} \rightarrow 1s_{1/2}(3E1)$ as a function of the nuclear charge. Upper panel: d_1 between $\widetilde{W}^{(\mathrm{LWA})}$ and $\widetilde{W}$ (dashed line), W (solid dark line), W_+ (solid blue line), $W^{(\mathrm{ZSL})}$ (dashed red line); middle panel: d_2 between W and $W^{(\mathrm{ZSL})}$ (solid green line); lower panel: $\phi(Z)$ is associated to $\widetilde{W}^{(\mathrm{LWA})}$ (dotted line), $\widetilde{W}$ (dashed line), W (solid dark line), W_+ (solid blue line), and $W^{(\mathrm{ZSL})}$ (dashed red line, Ref. [19]). Curves are drawn to guide the eye.

range $Z = 1$–20. Notably at the starting point $Z = 1$, the ZSL difference is $d_1^{(\mathrm{ZSL})} = 1.05\%$ whereas our relativistic and NRT-RC numbers are $d_1^{(\mathrm{R})} = 1.8 \times 10^{-2}\%$ and $d_1^{(\mathrm{RC})} = 2.3 \times 10^{-3}\%$, which illustrates how closely our DCGF approach

compares well with the two versions of the nonrelativistic approach.

(ii) To be more informative on the reliability of predictions, we plot in Fig. 1(c) the variation of the percent errors d_2 of

TABLE III. Three-photon decay rates in s^{-1} of combinations of $2E1E2$ and $2E2E1$ multipoles for the transitions $2s_{1/2} \rightarrow 1s_{1/2}$ and $2p_{1/2} \rightarrow 1s_{1/2}$, respectively, as a function of the nuclear charge. First entry: W; second entry: W_+; third entry: W_-; fourth entry: $\widetilde{W}$; fifth entry: $\widetilde{W}^{(\text{LWA})}$. Powers of ten are given in parentheses.

Z	$W(2E1E2)$	$W(2E2E1)$	Z	$W(2E1E2)$	$W(2E2E1)$	Z	$W(2E1E2)$	$W(2E2E1)$
1	3.277693(−14)	1.139904(−20)	35	8.387728(1)	3.655203(−2)	70	6.936210(4)	1.261596(2)
	3.277669(−14)	1.139896(−20)		8.312591(1)	3.625060(−2)		6.663111(4)	1.217161(2)
	5.608246(−37)	2.559297(−43)		3.838298(−9)	2.452990(−12)		3.483686(−3)	3.029391(−5)
	3.277860(−14)	1.139936(−20)		8.840371(1)	3.761398(−2)		8.462855(4)	1.434903(2)
	3.277920(−14)	1.139958(−20)		9.042298(1)	3.852170(−2)		9.259313(4)	1.577849(2)
5	3.195873(−7)	2.780158(−12)	40	3.119348(2)	1.785071(−1)	75	1.324185(5)	2.782625(2)
	3.195301(−7)	2.779700(−12)		3.082004(2)	1.765714(−1)		1.265871(5)	2.667309(2)
	2.142355(−24)	2.444452(−29)		4.705920(−8)	4.800707(−11)		1.292221(−2)	1.210431(−4)
	3.199617(−7)	2.781745(−12)		3.337284(2)	1.853909(−1)		1.664976(5)	3.238320(2)
	3.201094(−7)	2.783101(−12)		3.437149(2)	1.912532(−1)		1.845912(5)	3.610972(2)
10	3.256789(−4)	1.135162(−8)	45	9.879274(2)	7.199563(−1)	80	2.408690(5)	5.788423(2)
	3.254455(−4)	1.134414(−8)		9.731206(2)	7.099817(−1)		2.283530(5)	5.514756(2)
	5.620329(−19)	2.547438(−23)		3.987816(−7)	6.205913(−10)		3.837870(−2)	6.851647(−4)
	3.271874(−4)	1.137738(−8)		1.075289(3)	7.556768(−1)		3.130178(5)	6.921440(2)
	3.277920(−4)	1.139958(−8)		1.116152(3)	7.860299(−1)		3.519640(5)	7.833733(2)
15	1.863187(−2)	1.465050(−6)	50	2.756648(3)	2.494908	85	4.188488(5)	1.143922(3)
	1.860174(−2)	1.462872(−6)		2.704719(3)	2.452076		3.941845(5)	1.082655(3)
	8.482307(−16)	8.583036(−20)		2.791521(−6)	5.937305(−9)		3.503034(−1)	4.999190(−3)
	1.882380(−2)	1.472582(−6)		3.057116(3)	2.651101		5.653913(5)	1.410170(3)
	1.890214(−2)	1.479054(−6)		3.201094(3)	2.783101		6.453386(5)	1.621497(3)
20	3.272616(−1)	4.590827(−5)	55	6.936369(3)	7.644187	90	7.019176(5)	2.164816(3)
	3.263180(−1)	4.578659(−5)		6.777167(3)	7.482819		6.525950(5)	2.028963(3)
	1.520319(−13)	2.779302(−17)		1.861510(−5)	5.490398(−8)		9.343477(−1)	1.353255(−2)
	3.331904(−1)	4.633017(−5)		7.853383(3)	8.236125		9.855870(5)	2.753470(3)
	3.356590(−1)	4.669269(−5)		8.302813(3)	8.734563		1.142940(6)	3.219579(3)
25	3.005977	6.616057(−4)	60	1.601617(4)	2.114500(1)	95	1.135536(6)	3.925245(3)
	2.992395	6.588634(−4)		1.557488(4)	2.060216(1)		1.045678(6)	3.623710(3)
	8.359406(−12)	2.456880(−15)		9.367157(−5)	4.710968(−7)		6.384563	1.178928(−1)
	3.090229	6.712455(−4)		1.855103(4)	2.313961(1)		1.664322(6)	5.175828(3)
	3.126068	6.794680(−4)		1.982033(4)	2.481441(1)		1.962612(6)	6.159879(3)
30	1.830636(1)	5.829911(−3)	65	3.440175(4)	5.359065(1)	100	1.771644(6)	6.807850(3)
	1.818604(1)	5.794804(−3)		3.325718(4)	5.197598(1)		1.618206(6)	6.229189(3)
	2.642219(−10)	1.075139(−13)		8.946347(−4)	4.871306(−6)		3.409566(1)	4.068287(−1)
	1.903715(1)	5.952952(−3)		4.083420(4)	5.973916(1)		2.731221(6)	9.402125(3)
	1.935579(1)	6.058205(−3)		4.412980(4)	6.484093(1)		3.277920(6)	1.139958(4)

ZSL results for the $3E2$ multipole. It is obvious that with the growth of the nuclear charge, the DCGF and ZSL calculations agree with each other quite well. More precisely, as the nuclear charge grows larger, i.e., in the region $Z > 70$, the two methods agree to within 0.5%.

(iii) Switching our attention to the $3E1$ multipole in Fig. 1(d), one observes an overlap region of the two schemes for low and medium nuclear charges $Z \leqslant 40$. There the percent error is stabilized to within $d_2 = 8 \times 10^{-2}\%$. Then it starts increasing and rather rapidly for heavy ions with $Z \geqslant 70$. It gets worse at $Z = 95$ where it experiences a 2% divergence.

(iv) The general trend of the curves in Figs. 1(a) and 1(b) is relevant to the fact that relativistic effects increase smoothly except for $3E2$ of ZSL as mentioned above, and become substantial with the nuclear charge. It is also apparent that interferences between the nonnegative and negative parts of

the complete set of relativistic Sturmian functions of the first order are more important in the $3E2$ channel.

(v) As evident in Figs. 1(e) and 1(f), corrections arising from relativity in the normalized integrated emission rate $\phi(Z)$ manifest themselves in the same way as in the case of two-photon decays studied in detail in Ref. [18].

(vi) Finally, in the NRT-RC approach, we employ a length transition operator that includes nondipole corrections, and acting on the Schrödinger-Coulomb Sturmian wave functions in the matrix elements. In comparison to NRT-LWA, one sees in Figs. 1(a), 1(b), 1(e), and 1(f) a significant improvement in the NRT-RC results, particularly for $3E2$. Thus introducing nondipole effects in the transition operator gives better results.

As a further step for more investigations of three-photon decays, we present in Table III data of our computations for $2s_{1/2} \rightarrow 1s_{1/2}(2E1E2)$ and $2p_{1/2} \rightarrow 1s_{1/2}(2E2E1)$ transitions and for Z ranging from 1 to 100. The corresponding
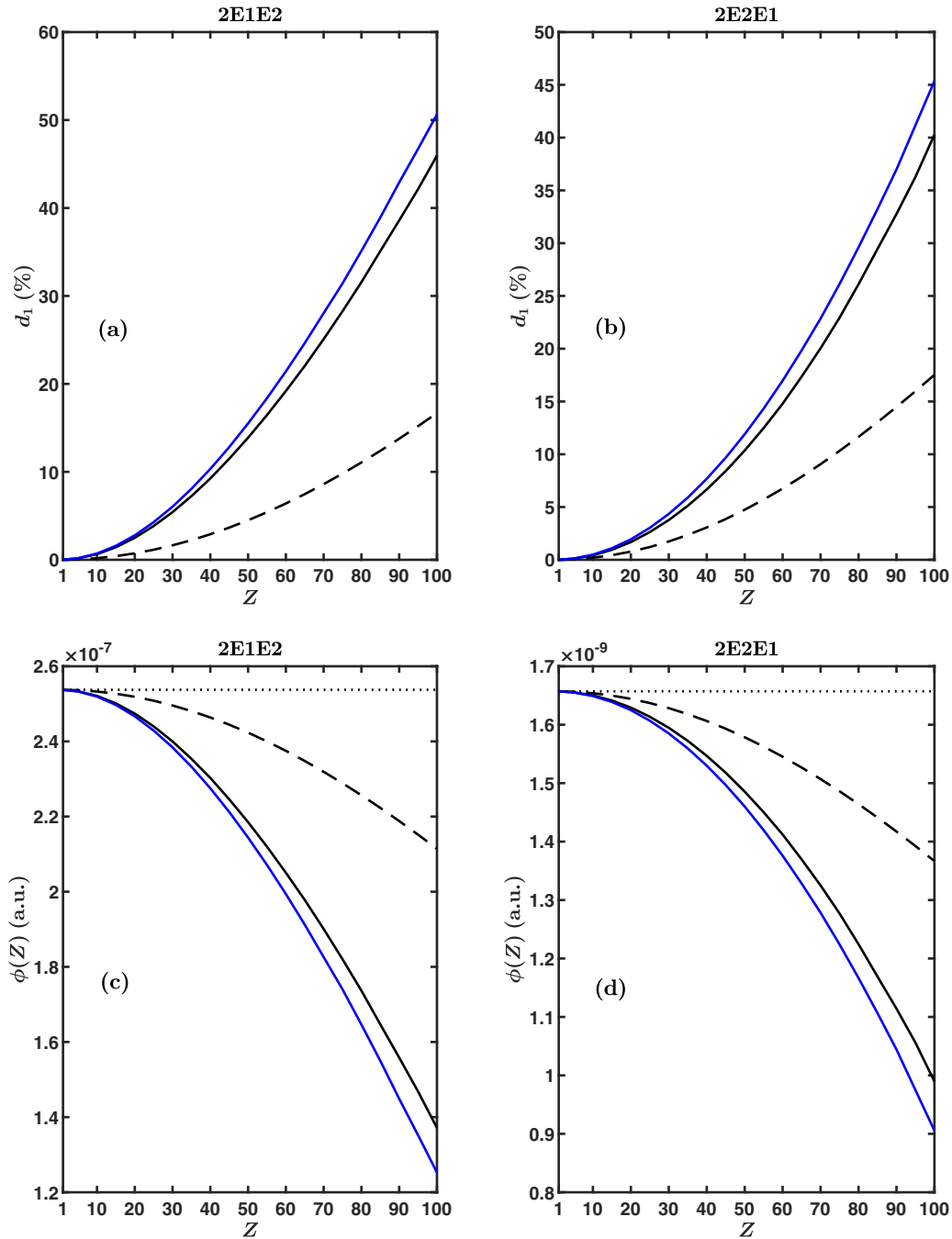
FIG. 2. An illustration of the behavior of the percentage difference and the normalized integrated decay rate for the transitions $2s_{1/2} \to 1s_{1/2}(2E1E2)$ and $2p_{1/2} \to 1s_{1/2}(2E2E1)$ as a function of the nuclear charge. Upper panel: d_1 between $\widetilde{W}^{(\text{LWA})}$ and $\widetilde{W}$ (dashed line), W (solid dark line), W_+ (solid blue line); lower panel: $\phi(Z)$ is associated to $\widetilde{W}^{(\text{LWA})}$ (dotted line), $\widetilde{W}$ (dashed line), W (solid dark line), and W_+ (solid blue line). Curves are drawn to guide the eye.

percentage differences, normalized integrated decay rates and single differential probabilities as defined previously are displayed in Figs. 2 and 3. The plots clearly depict the features and tendencies that are mentioned above with, however, a marked difference. The overall influence of retardation as well as the effects of the negative spectrum of the Sturmian basis are less significant. The shapes as well as the maxima of the spectral distributions in Fig. 3 are almost the same at $Z = 25$, 50, 75, and 100. The curves of NRT-LWA and NRT-RC are peaked at $y_{\text{max}} = 0.313$ whatever the nuclear charge. For the

relativistic schemes, the maximum is slightly shifted at $y_{\text{max}} = 0.327$ for $Z = 75$ and 100, which is close to the value $1/3$ of the energy equipartition. It is worth noting that the emission spectra are not symmetric due to a small tail at their right-hand side. To end, let us underline that relativistic corrections make the single differential probabilities less sharp and reduce their intensities.

We also check in this work the Bose-Einstein statistics in the emission processes under consideration. It is lengthily discussed by Zalialiutdinov *et al.* in Refs. [20,21]. According to
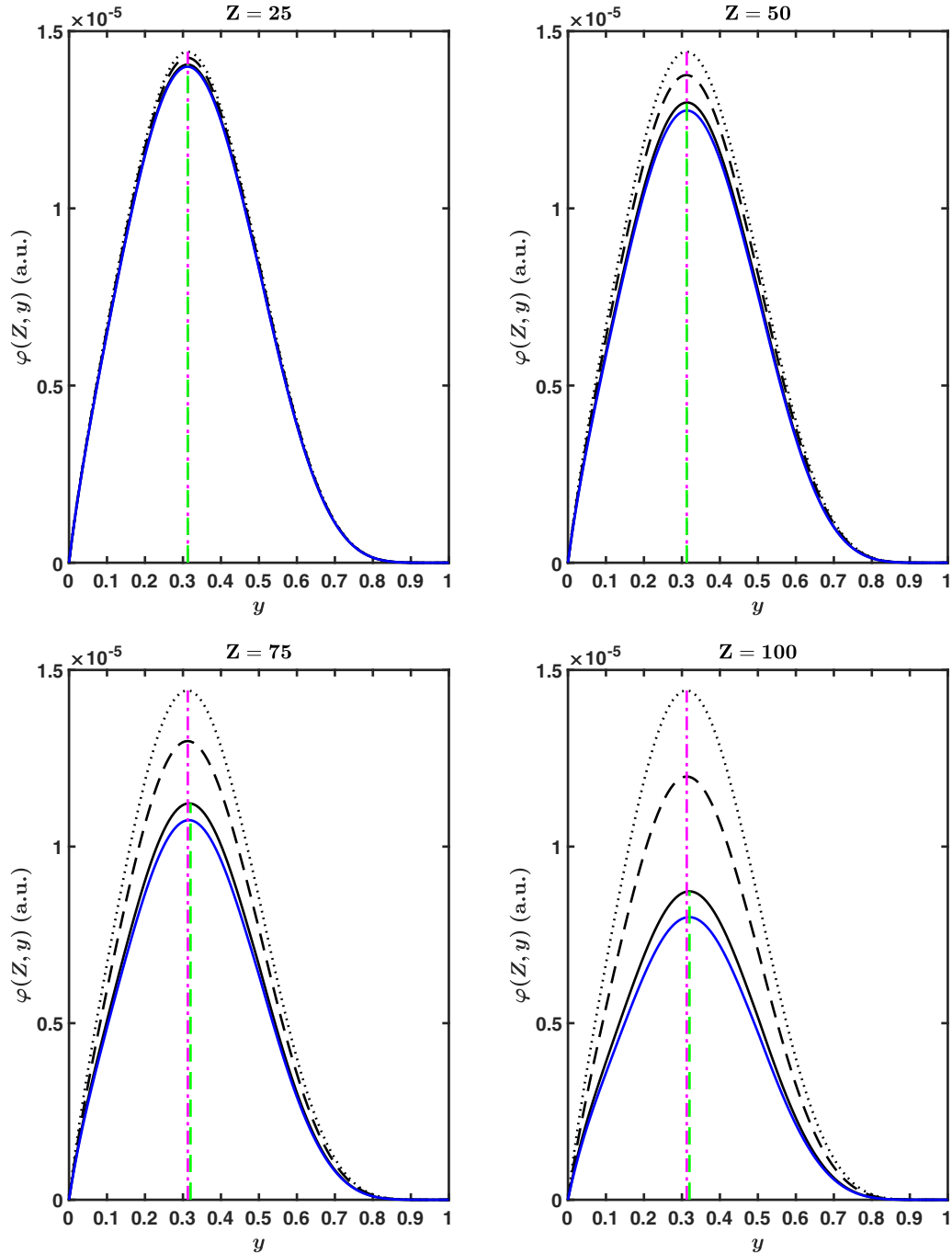
FIG. 3. Single differential probabilities for the transition $2p_{1/2} \to 1s_{1/2}(2E2E1)$ versus the energy fraction of a photon and for the nuclear charges $Z = 25$, 50, 75 and 100. $\varphi(Z, y)$ is associated to $\widetilde{W}^{(\text{LWA})}$ (dotted line), $\widetilde{W}$ (dashed line), W (solid dark line), and W_+ (solid blue line). The dashed purple and green vertical lines indicate the maxima of the nonrelativistic and relativistic results respectively. Curves are drawn to guide the eye.

the so-called second spin-statistics selection rule (SSSR-2) established by these authors, three equivalent photons involved in any atomic transition can only have odd values for the total angular momentum. Note that equivalent photons are of the same type with equal frequencies and equal angular momenta. This exclusion principle for photons is confirmed in Fig. 4 where are depicted double differential probabilities of some three-dipole-photon hyperfine transitions versus energy

fractions y_1 and y_2 at $Z = 100$. Figures 4(b) and 4(d) are two-dimensional (2D) sectional cuts at $y_2 = 1/3$ of Figs. 4(a) and 4(c) for the transitions $2p_{3/2}(F_i = 0) \to 2s_{1/2}(F_f = 2)$ and $2p_{3/2}(F_i = 2) \to 2s_{1/2}(F_f = 0)$, respectively. The nuclear spins are $3/2$ in the first and $1/2$ in the second. These 2D curves exhibit a pit at the bottom of which lies the lowest zero point with the abscissa $y_1 = 1/3$. In other words, for the even value 2 of the total angular momentum of
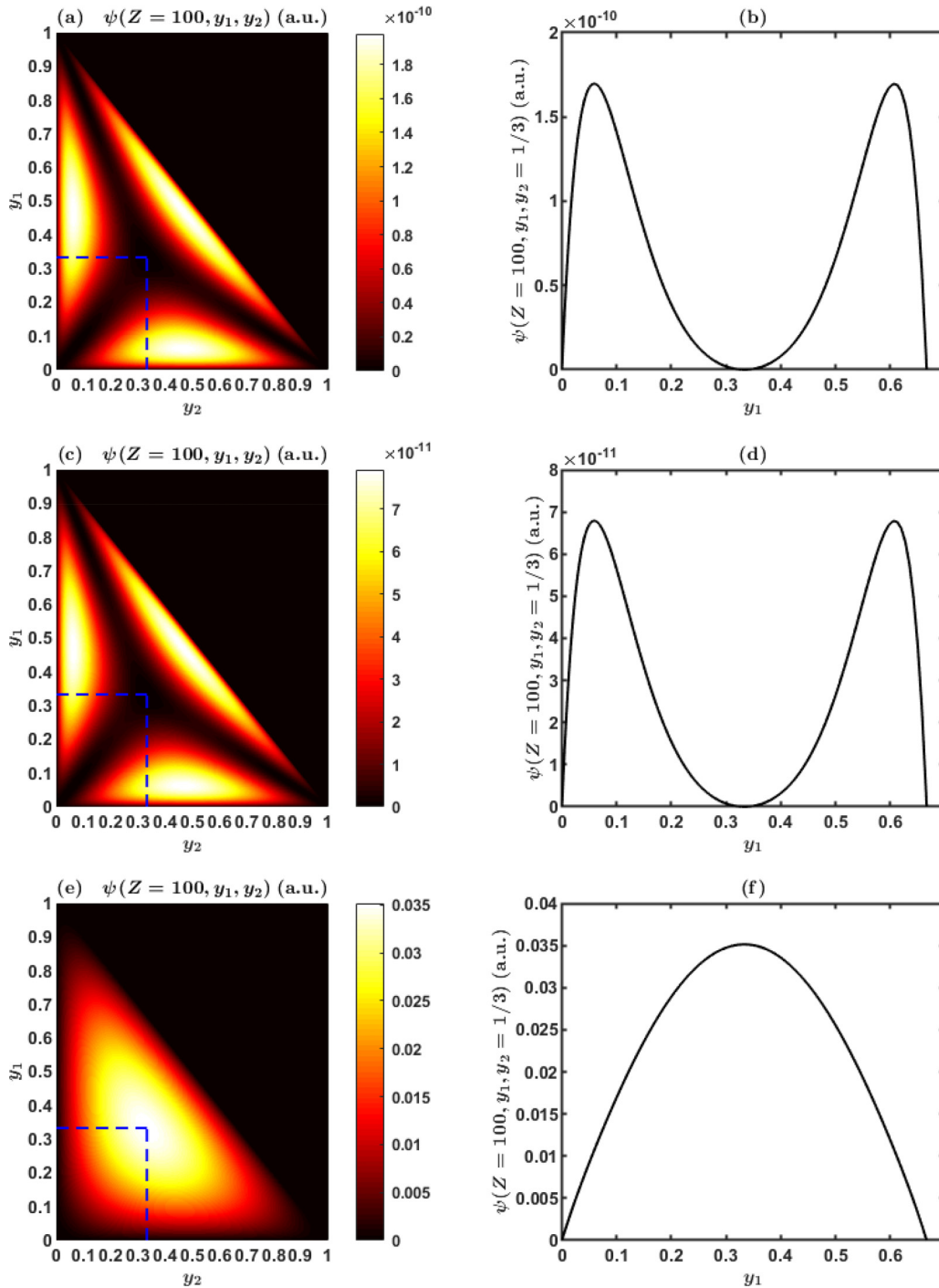
FIG. 4. Double differential probabilities $\psi(Z = 100, y_1, y_2)$ versus photon energy fractions y_1 and y_2 (left column) and two-dimensional sectional cuts at $y_2 = 1/3$ (right column) for $Z = 100$ and $3E1$ multipole. Upper panel: $2p_{3/2}(F_i = 0) \rightarrow 2s_{1/2}(F_f = 2)$ with $I = 3/2$; middle panel: $2p_{3/2}(F_i = 2) \rightarrow 2s_{1/2}(F_f = 0)$ with $I = 1/2$; lower panel: $2p_{1/2}(F_i = 1) \rightarrow 1s_{1/2}(F_f = 0)$ with $I = 1/2$. The dashed blue lines indicate the mimima for (a) and (c), and the maximum for (e). Curves are drawn to guide the eye.

three-photon system, the decay probabilities turn to zero when the energy fractions of the emitted photons are equal. Switching our attention to Figs. 4(e) and 4(f) for the transition $2p_{1/2}(F_i = 1) \rightarrow 1s_{1/2}(F_f = 0)$ with $I = 1/2$, as expected, one sees a hump in the 2D distribution with a maximum at $y_1 = 1/3$. Thus, unlike the foregoing case, the odd value 1 of the total angular momentum is not forbidden according to the SSSR-2.

V. CONCLUDING REMARKS

The purpose of this work was first to extend the DCGF approach previously developed for 2-PRT to 3-PRT, and second to assess the effectiveness and usefulness of our scheme for H-like ions with nuclear charge values ranging from 1 to 100. To this end, we have formulated a general analytical relativistic theory of spectral distributions and total decay

rates for atomic systems with either a spinless nucleus or a nonzero nuclear spin. Moreover, we have derived explicitly two other nonrelativistic limiting cases to evaluate the relativistic effects, the influence of the negative spectrum of the Sturmian basis, and the effects of nondipole corrections incorporated in the transition operator. These approaches have been applied with a great care to four electric multipole channels, namely, $3E1$, $3E2$, $2E1E2$, and $2E2E1$. Then, our numerical results have been compared to those obtained by the group of Zalialiutdinov. It emerges that the degree of agreement between the two computations is quite satisfactory except at low and high nuclear charges for the $3E2$ and $3E1$ channels, respectively. Finally, we have checked the validity of the SSSR-2 for three equivalent photons. We are, at present, using this extended model for extensive applications to transitions involving magnetic multipoles. This work will be reported in a forthcoming paper.

ACKNOWLEDGMENTS

APPENDIX: EVALUATION OF SPIN-ANGULAR COUPLING FACTORS INVOLVING SUMS OF PRODUCTS OF SIX WIGNER-$3j$-SYMBOLS

Spin-angular coupling factors (SACF) that occur in transition matrix elements of the right hand side of Eq. (1) as cumbersome sums of products of six $3j$ symbols, are written

$$\Theta_{j_1 j_2}^{j_1' j_2'}[(w, v, u), (w', v', u')]$$
$$= \sum_{m_i m_f} \sum_{\text{all } M} \theta_{j_1 j_2}(w, v, u)\theta_{j_1' j_2'}(w', v', u'), \quad \text{(A1)}$$

where $\{u, v, w, u', v', w' = 1, 2, 3\}$. They can be conveniently cast into analytical forms suitable for numerical computations. Thus, by using sum rules of $3j$ symbols and Clebsch-Gordan coefficients [38], and after lengthy calculations and simplifications, we find the following expressions of the possible 21 SACF.

(i) Six direct terms of identical pairs of triple endexes $\{(w, v, u), (w, v, u)\}$

$$\Theta_{j_1 j_2}^{j_1' j_2'}[(w, v, u), (w, v, u)] = \delta_{j_1 j_1'} \delta_{j_2 j_2'}, \quad \text{(A2)}$$

where $\delta_{j j'}$ is the Kronecker's symbol.

(ii) Three cross terms of circular-circular type

$$\Theta_{j_1 j_2}^{j_1' j_2'}[(3, 2, 1), (1, 3, 2)] = \hat{K}_{j_1 j_1'}^{(1)}(2, 1)\check{K}_{j_2 j_2'}^{(2)}(3, 1), \quad \text{(A3)}$$

$$\Theta_{j_1 j_2}^{j_1' j_2'}[(3, 2, 1), (2, 1, 3)] = \hat{K}_{j_1 j_1'}^{(2)}(3, 1)\check{K}_{j_2 j_2'}^{(1)}(3, 2), \quad \text{(A4)}$$

$$\Theta_{j_1 j_2}^{j_1' j_2'}[(1, 3, 2), (2, 1, 3)] = \hat{K}_{j_1 j_1'}^{(1)}(3, 2)\check{K}_{j_2 j_2'}^{(2)}(1, 2). \quad \text{(A5)}$$

(iii) Three cross terms of noncircular-noncircular type

$$\Theta_{j_1 j_2}^{j_1' j_2'}[(3, 1, 2), (2, 3, 1)] = \hat{K}_{j_1 j_1'}^{(1)}(1, 2)\check{K}_{j_2 j_2'}^{(2)}(3, 2), \quad \text{(A6)}$$

$$\Theta_{j_1 j_2}^{j_1' j_2'}[(3, 1, 2), (1, 2, 3)] = \hat{K}_{j_1 j_1'}^{(2)}(3, 2)\check{K}_{j_2 j_2'}^{(1)}(3, 1), \quad \text{(A7)}$$

$$\Theta_{j_1 j_2}^{j_1' j_2'}[(2, 3, 1), (1, 2, 3)] = \hat{K}_{j_1 j_1'}^{(1)}(3, 1)\check{K}_{j_2 j_2'}^{(2)}(2, 1). \quad \text{(A8)}$$

(iv) Nine cross terms of circular-noncircular type

$$\Theta_{j_1 j_2}^{j_1' j_2'}[(3, 2, 1), (3, 1, 2)] = \hat{K}_{j_1 j_1'}^{(1)}(2, 1)\delta_{j_2 j_2'},$$

$$\Theta_{j_1 j_2}^{j_1' j_2'}[(1, 3, 2), (1, 2, 3)] = \hat{K}_{j_1 j_1'}^{(1)}(3, 2)\delta_{j_2 j_2'}, \quad \text{(A9)}$$

$$\Theta_{j_1 j_2}^{j_1' j_2'}[(2, 1, 3), (2, 3, 1)] = \hat{K}_{j_1 j_1'}^{(1)}(1, 3)\delta_{j_2 j_2'},$$

$$\Theta_{j_1 j_2}^{j_1' j_2'}[(3, 2, 1), (2, 3, 1)] = \delta_{j_1 j_1'}\check{K}_{j_2 j_2'}^{(1)}(3, 2), \quad \text{(A10)}$$

$$\Theta_{j_1 j_2}^{j_1' j_2'}[(1, 3, 2), (3, 1, 2)] = \delta_{j_1 j_1'}\check{K}_{j_2 j_2'}^{(1)}(1, 3),$$

$$\Theta_{j_1 j_2}^{j_1' j_2'}[(2, 1, 3), (1, 2, 3)] = \delta_{j_1 j_1'}\check{K}_{j_2 j_2'}^{(1)}(2, 1), \quad \text{(A11)}$$

$$\Theta_{j_1 j_2}^{j_1' j_2'}[(3, 2, 1), (1, 2, 3)] = K_{j_1 j_2 j_1' j_2'}(3, 2, 1),$$

$$\Theta_{j_1 j_2}^{j_1' j_2'}[(1, 3, 2), (2, 3, 1)] = K_{j_1 j_2 j_1' j_2'}(1, 3, 2), \quad \text{(A12)}$$

$$\Theta_{j_1 j_2}^{j_1' j_2'}[(2, 1, 3), (3, 1, 2)] = K_{j_1 j_2 j_1' j_2'}(2, 1, 3). \quad \text{(A13)}$$

The angular factors $\hat{K}$, $\check{K}$, and K are given by

$$\hat{K}_{j_1 j_1'}^{(1)}(v, u) = (-1)^\varphi [j_1, j_1']^{1/2} \begin{Bmatrix} j_2 & j_1' & L_u \\ j_i & j_1 & L_v \end{Bmatrix}, \quad \text{(A14)}$$

$$\hat{K}_{j_1 j_1'}^{(2)}(v, u) = (-1)^\varphi [j_1, j_1']^{1/2} \begin{Bmatrix} j_2' & j_1' & L_u \\ j_i & j_1 & L_v \end{Bmatrix}, \quad \text{(A15)}$$

$$\check{K}_{j_2 j_2'}^{(1)}(v, u) = (-1)^\varphi [j_2, j_2']^{1/2} \begin{Bmatrix} j_f & j_2' & L_u \\ j_1 & j_2 & L_v \end{Bmatrix}, \quad \text{(A16)}$$

$$\check{K}_{j_2 j_2'}^{(2)}(v, u) = (-1)^\varphi [j_2, j_2']^{1/2} \begin{Bmatrix} j_f & j_2' & L_u \\ j_1' & j_2 & L_v \end{Bmatrix}, \quad \text{(A17)}$$

$$K_{j_1 j_2 j_1' j_2'}(w, v, u) = [j_1, j_2, j_1', j_2']^{1/2} \begin{Bmatrix} L_w & j_2 & j_f \\ j_i & j_1 & L_u \\ j_1' & L_v & j_2' \end{Bmatrix}, \quad \text{(A18)}$$

where $\varphi = L_u + L_v + 1$.

[1] A. Surzhykov, P. Indelicato, J. P. Santos, P. Amaro, and S. Fritzsche, Phys. Rev. A **84**, 022511 (2011).

[2] R. Marrus and R. W. Schmieder, Phys. Rev. A **5**, 1160 (1972).

[3] *Laser Spectroscopy of Atoms and Molecules*, edited by H. Walther (Springer-Verlag, Berlin, 1976).

[4] R. J. Fonck, D. H. Tracy, D. C. Wright, and F. S. Tomkins, Phys. Rev. Lett. **40**, 1366 (1978).

[5] Z. Zheng, A. M. Weiner, J. H. Marsh, and M. M. Karkhanehchi, IEEE Photon. Technol. Lett. **9**, 493 (1997).

[6] S. Paul and Y. K. Ho, Phys. Rev. A **79**, 032714 (2009).

[7] L. Safari, P. Amaro, S. Fritzsche, J. P. Santos, and F. Fratini, Phys. Rev. A **85**, 043406 (2012).

[8] G. Breit and E. Teller, Astrophys. J. **91**, 215 (1940).

[9] M. Göppert-Mayer, Ann. Phys. (Leipzig) **401**, 273 (1931).

[10] S. P. Goldman and G. W. F. Drake, Phys. Rev. A **24**, 183 (1981).

[11] G. W. F. Drake and S. P. Goldman, Phys. Rev. A **23**, 2093 (1981).

[12] J. P. Santos, F. Parente, and P. Indelicato, Eur. Phys. J. D **3**, 43 (1998).

[13] P. Amaro, J. P. Santos, F. Parente, A. Surzhykov, and P. Indelicato, Phys. Rev. A **79**, 062504 (2009).

[14] U. D. Jentschura and A. Surzhykov, Phys. Rev. A **77**, 042507 (2008).

[15] L. N. Labzowsky and A. V. Shonin, Phys. Lett. A **333**, 289 (2004).

[16] L. Labzowsky, A. V. Shonin, and D. A. Solovyev, J. Phys. B: At. Mol. Opt. Phys. **38**, 265 (2005).

[17] L. Labzowsky, D. Solovyev, G. Plunien, and G. Soff, Eur. Phys. J. D **37**, 335 (2006).

[18] Z. Bona, H. M. Tetchou Nganso, T. B. Ekogo, and M. G. Kwato Njock, Phys. Rev. A **89**, 022514 (2014).

[19] T. Zalialiutdinov, D. Solovyev, and L. Labzowsky, J. Phys. B: At. Mol. Opt. Phys. **49**, 055001 (2016).

[20] T. Zalialiutdinov, D. Solovyev, L. Labzowsky, and G. Plunien, Phys. Rev. A **91**, 033417 (2015)

[21] T. A. Zalialiutdinov, D. A. Solovyev, L. N. Labzowsky, and G. Plunien, Phys. Rep. **737**, 1 (2018).

[22] D. DeMille, D. Budker, N. Derr, and E. Deveney, Phys. Rev. Lett. **83**, 3978 (1999).

[23] R. W. Dunford, Phys. Rev. A **69**, 062502 (2004).

[24] D. Angom, K. Bhattacharya, and S. D. Rindani, Int. J. Mod. Phys. A **22**, 707 (2007).

[25] M. G. Kozlov, D. English, and D. Budker, Phys. Rev. A **80**, 042504 (2009).

[26] D. English, V. V. Yashchuk, and D. Budker, Phys. Rev. Lett. **104**, 253604 (2010).

[27] *Handbook of Atomic Molecular and Optical Physics*, edited by G. W. F. Drake (Springer, New York, 2006).

[28] A. I. Akhiezer and V. B. Berestetskii, *Quantum Electrodynamics* (Wiley, New York, 1965).

[29] R. Szmytkowski, J. Phys. B: At. Mol. Opt. Phys. **30**, 825 (1997); **30**, 2747(E) (1997).

[30] L. Armstrong, W. R. Fielder, and D. L. Lin, Phys. Rev. A **14**, 1114 (1976).

[31] I. P. Grant, J. Phys. B: At. Mol. Phys. **7**, 1458 (1974).

[32] L. Hostler and R. H. Pratt, Phys. Rev. Lett. **10**, 469 (1963).

[33] A. Maquet, Phys. Rev. A **15**, 1088 (1977).

[34] R. A. Swainson and G. W. F. Drake, J. Phys. A: Math. Gen. **24**, 79 (1991); **24**, 95 (1991); **24**, 1801 (1991).

[35] *Handbook of Mathematical Functions*, NBS Applied Mathematical Series, edited by M. Abramowitz and I. A. Stegun (National Bureau of Standards, Washington, D.C., 1985).

[36] I. S. Gradshteyn and I. M. Ryzhik, *Table of Integrals, Series and Products, Seventh Edition*, edited by A. Jeffrey and D. Zwillinger (Academic Press, New York, 2007).

[37] L. Spitzer and J. L. Greenstein, Astrophys. J. **114**, 407 (1951).

[38] D. A. Varshalovich, A. N. Moskalev, and V. K. Khersonskii, *Quantum Theory of Angular Momentum* (World Scientific, Singapore, 1988).